Keldysh Institute • Publication search

Keldysh Institute preprints • Preprint No. 69, 2022

ISSN 2071-2898 (Print)
ISSN 2071-2901 (Online)

G.V. Shpatakovskaya

Atomic number similarity law in individual electronic shells of all natural elements

Recommended form of bibliographic references: Shpatakovskaya G.V. Atomic number similarity law in individual electronic shells of all natural elements // Keldysh Institute Preprints. 2022. No. 69. 14 p.
https://doi.org/10.20948/prepr-2022-69-e
https://library.keldysh.ru/preprint.asp?id=2022-69&lg=e

KELDYSH INSTITUTE OF APPLIED MATEMATICS
Russian Academy of Sciences

G.V.Shpatakovskaya

Atomic number similarity law in individual electronic shells of all natural elements

Moscow — 2022

Galina Vasil'evna Shpatakovskaya

Atomic number similarity law in individual electronic shells of all natural elements

Experimental data on the electronic binding energies in individual *K, L, M, N, O, P* shells for all atoms from hydrogen to uranium are analyzed using special reduced coordinates. The atomic number similarity law is revealed in every subshell and it is expressed through two smooth functions. The violation of smoothness usually indicates measurement errors and a change in slope indicates a filling subshell. The polynomial approximation of the functions allows to recover missing or erroneous data with an accuracy of 1–2%.

Key words: periodic table of elements, orbital energy, electron binding energy, electron shell, atomic number self-similarity, semi-classical method.

Шпаковская Г.В.

Закон подобия по атомному номеру в отдельных электронных оболочках всех естественных элементов

Экспериментальные данные по электронным энергиям связи в отдельных *K, L, M, N, O, P* оболочках для всех атомов от водорода до урана проанализированы в специальных приведенных координатах. В каждой под-оболочке обнаружен закон подобия по атомному номеру, который выражается через две монотонные функции. Нарушение монотонности указывает на ошибки измерения, а изменение наклона свидетельствует о заполнении под-оболочки. Полиномиальная аппроксимация этих функций позволяет восстанавливать отсутствующие или ошибочные данные с точностью 1–2%.

Ключевые слова: периодическая таблица элементов, орбитальная энергия, энергия связи электрона, электронная оболочка, подобие по атомному номеру, квазиклассический метод

1 Introduction

The data on electron orbital binding energies in atoms are necessary for many applications: optic and x-ray research methods, scattering problems, astrophysics and so on. One can use theoretical results (for example, [1, 2]) or experimental measurements [3, 4, 5] as a source of the data. But a comparison of different data sources reveals lack or scatter of experimental data, difference between experiment and theory [6]. In the latter case, the question arises about the reason for the difference: is this an inaccuracy of measurement or is some effect not taken into account in the theory? Obviously, the binding energy dependence on the atomic number Z could provide an answer to this question.

In our previous paper [7], a semiclassical method was proposed to find such dependence. Application of the method to the analysis of K and L shells in many-electron atoms ($Z \geq 10$) [8] revealed a similarity in the atomic number of measured electronic orbital energies and made it possible not only to describe experimental K, L_I, L_{II}, L_{III} X-ray levels with an accuracy better than one percent but also to control their reliability. The method has shown its efficiency in the analysis of the internal and outer electron shells of lanthanides [9], detected patterns in the measured first ionization potentials of lanthanides and actinides [10].

In present paper we apply the method to study the available experimental and some theoretical electronic binding energies in all natural atoms of the periodic table ($1 \leq Z \leq 92$). Our goal is to show the general picture of the dependence of the measured binding energies on the atomic number in individual electron subshells, detect patterns and explain deviations from them and thus provide a way to recover missing or erroneous data.

We use experimental data on binding energies for elements in their natural forms which are summarized in the booklet [3] and theoretical orbital energies calculated by relativistic local density approximation (RLDA) [2] from the database [11]. Experimental data from other sources [4, 5] are used also for comparison.

The base of experimental binding energies [3] was chosen as the main one, since it contains data for all natural elements, but these data are taken from the publications 40–50 years ago. In database [5], the orbital binding energies for all elements from hydrogen to lawrencium (Z = 103) are given, but there are no references to sources and the spin-orbit interaction is not taken into account. The most recent and accurate data can be found in database [4], but they are not available for all atoms and not for all subshells.

As far as theoretical models are concerned, the multi-configuration Dirac–Fock method (MCDF) [1] is considered more accurate for such calculations, but its application to middle and outer shells for all atoms has not yet been implemented.

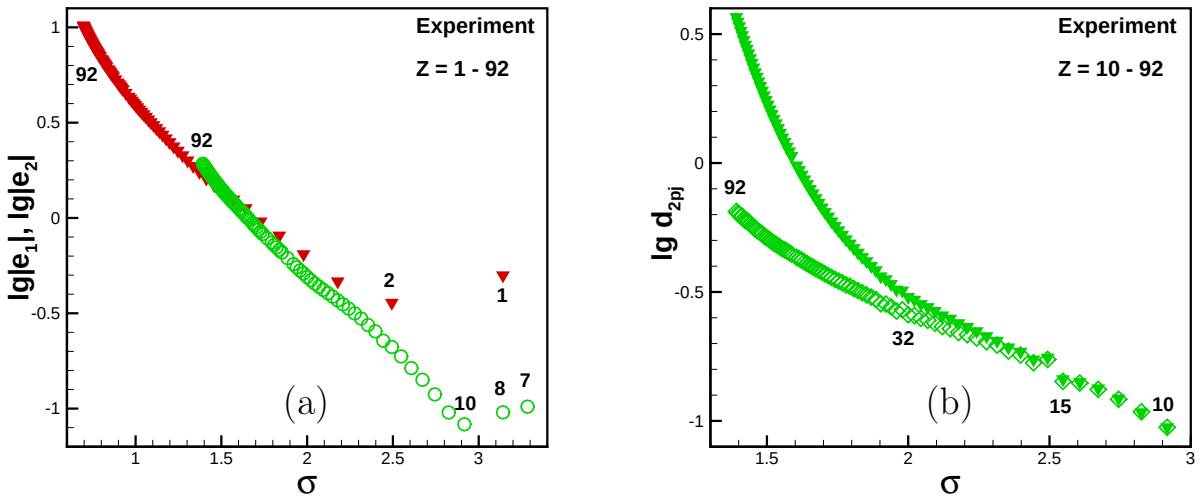

Fig. 1: The functions $\lg|\mathrm{e}_1(\sigma_1)|$ (red solid $\bigtriangledown$), $\lg|\mathrm{e}_2(\sigma_2)|$ (green open $\circ$) (**a**) and $\lg \mathrm{d}_{2p1/2}(\sigma_2)$ (green open $\diamondsuit$), $\lg \mathrm{d}_{2p3/2}(\sigma_2)$ (green solid $\bigtriangleup$) according to the data from [3] (**b**).

The results [11] of the RLDA model [2] used by us cannot be considered standard, but their advantage is in the completeness of information for all shells of all atoms from hydrogen to fermium (Z = 100) with allowance for relativistic effects.

In section 2 there are experimental K, L, M shells analysis. In section 3 experimental data in N, O and P shells from [3] compare with RLDA results. In section 4 polynomial interpolations are used to approximate experimental binding energies and the estimates obtained are compared with experimental data from other sources.

2 Experimental electron binding energies in the K, L and M shells

To analyze a large array of data on the orbital binding energies of many atoms, special reduced values in atomic units ($\hbar = m_e = e = 1$) are used:

$$\mathrm{e}_n = E_{n0} Z^{-4/3}, \quad \sigma_n = \pi n Z^{-1/3}, \tag{1}$$

$$\mathrm{d}_{nlj} = (E_{nlj} - E_{n0})/Z^{2/3}/\lambda^2. \tag{2}$$

Here E_{nlj} is orbital energy level in atomic units (the binding energy is $|E_{nlj}|$), n, l, j are quantum numbers, E_{n0} is an electronic energy in s-state ($l = 0$), $\lambda = l + 1/2$, $j = l \mp 1/2$ is a total electron momentum with account for a relativistic spin-orbital interaction.

Expressions (1), (2) were prompted by the form of the dependence on the atomic number of the orbital energy levels in the Thomas–Fermi (TF) atom. When deriving the latter, the Bohr–Sommerfeld quantization condition was used (for more details see [7]). In accordance with our method, we assign pairs of quantities: $e_n - \sigma_n, \quad d_{nlj} - \sigma_n$ and thus construct the dependence $\mathrm{e}_n(\sigma_n)$ and $\mathrm{d}_{nlj}(\sigma_n)$. In the TF atom, the functions $\mathrm{e}(\sigma)$ and $\mathrm{d}(\sigma)$ do not depend on quantum numbers; they are universal and are calculated from the TF potential.

The functions $\mathrm{e}_1(\sigma_1)$ and $\mathrm{e}_2(\sigma_2)$ are shown in figure 1(a) on a semilog scale. Numbers under or above a symbol in this and further figures mean the atomic number Z. Compared to the article [8], light elements ($1 \le Z \le 9$) are also considered. Both functions are smooth except $\lg|\mathrm{e}_1|$ for $Z = 1$ and $\lg|\mathrm{e}_2|$ for $Z = 7, 8$. Deviation in the first case corresponds to unfilled K shell, in the second case to unfilled L shell.

The smooth behavior is also confirmed in figure 1(b) for the functions $\lg \mathrm{d}_{2p1/2}(\sigma_2)$ and $\lg \mathrm{d}_{2p3/2}(\sigma_2)$ except for $Z = 15, 16, 32$. In contrast to [8], where the functions $\lg \mathrm{d}_{2pj}$ were built based on data for only 11 elements, figure 1(b) shows the results for all elements from neon to uranium. The influence of relativistic spin-orbital interaction is clearly visible, which increases with increasing atomic number (from right to left).

Figure 2(a) shows the function $\lg|\mathrm{e}_3(\sigma_3)|$ for all elements $18 \le Z \le 92$, with main and different transition atomic groups denoted by different colors and symbols. One can see their continuous smooth behavior. However unlike 1s and 2s curves (see figure 1(a)) there are sharp bends near $Z = 20$ and $Z = 28$. The change in the slope coincides with the position of the iron group $21 \le Z \le 28$ in which the 3d subshell is filling.

In figure 2(b) functions $\lg \mathrm{d}_{3pj}(\sigma_3)$, $j = 1/2,\ 3/2$ are shown. Compared to the behavior of an overall smooth function, there are some points ($Z = 27$, 31, 37, 43, 56, 59, 68, 84) falling out of continuous dependence. It is assumed that the reason for these deviations is inaccuracy of measurements.

3 Experimental and theoretical binding energies in N, O, P shells

In the previous section 2, it was shown that the filling of $3d$ states in the first transition iron group was expressed in a change in the slope of the function

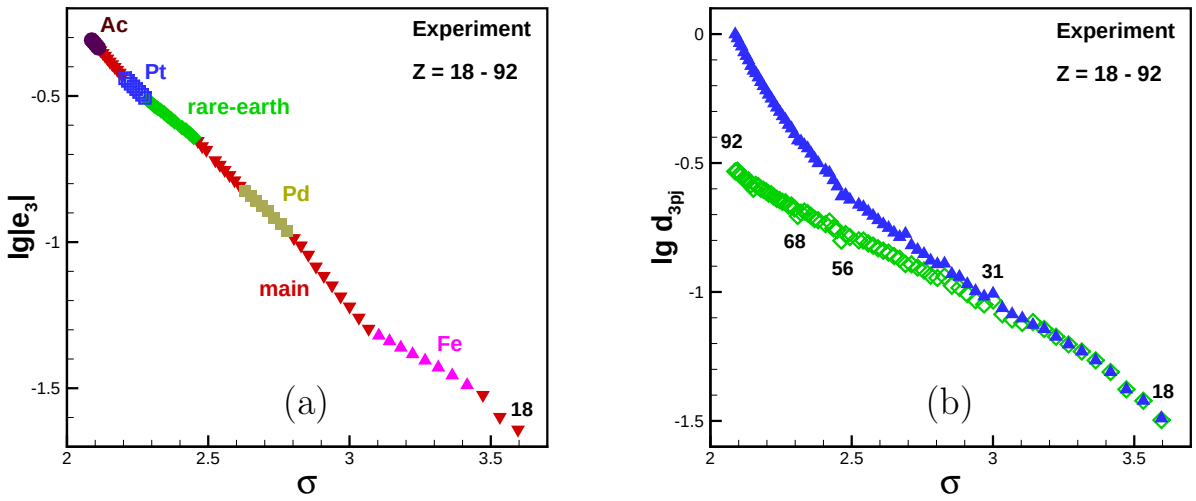

Fig. 2: The function $\lg|e_3(\sigma_3)|$ for different atomic groups, denoted by different colors and symbols: main (red solid $\bigtriangledown$), Fe (pink solid $\bigtriangleup$), Pd (khaki solid $\triangleleft$), rare-earth (green solid $\diamondsuit$), Pt (blue open square), Ac (brown solid $\circ$)(**a**) and functions $\lg d_{3p1/2}(\sigma_3)$ (green open $\diamondsuit$), $\lg d_{3p3/2}(\sigma_3)$ (blue solid $\bigtriangleup$) according to the data from [3] (**b**).

$\lg|e_3(\sigma_3)|$. Figure 3(a) reflects the change in the slope of the $\lg|e_4(\sigma_4)|$ dependence where the 4d states are filling in the palladium transition group. In figure 3(b) the experimental function $e_4(\sigma_4)$ is shown again in comparison with the theoretical results by RLDA [2, 11]. The smooth behavior of both curves and some discrepancy between the theoretical and experimental values are seen.

The same figure 3(b) shows theoretical and experimental functions $d_{4pj}(\sigma_4)$. Both RLDA curves turn out to be perfectly smooth and their behavior contrasts with the chaotic spread of experimental data for 4p1/2 energies of the rare-earth elements ($57 \le Z \le 70$). The coincidence of the experimental energies E_{4pj} for different j in the range $48 \le Z \le 54$ is also in doubt.

Analogous consideration of the theoretical and experimental data is presented in figures 4 for the 5s and 5pj energies in the elements from xenon to uranium. In figure 4(a), there is a deviation from the general dependence for the osmium atom ($Z = 76$). The most chaotic scatter of points is again visible in the region of rare-earth elements. This scatter, due to relation (2), also manifests itself in the scatter of points $\lg d_{5pj}(\sigma_5)$ in figure 4(b). There are also some disruptions in the theoretic curve $\lg|e_5(\sigma_5)|$ at $Z = 57, 58, 64$. These and the deviations described

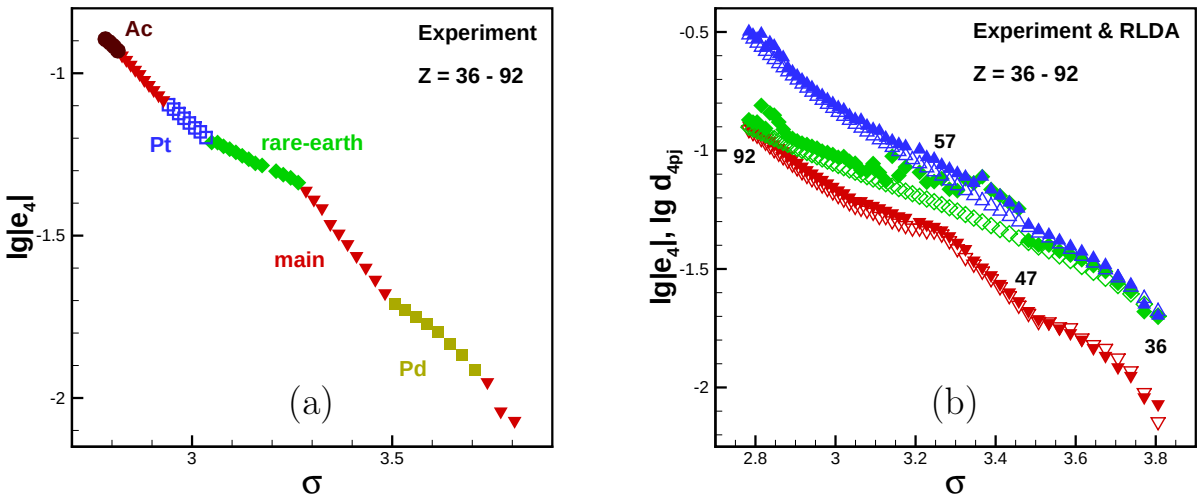

Fig. 3: The function $\lg|\mathrm{e}_4(\sigma_4)|$ for different atomic groups, denoted by different colors and symbols: main (red solid $\bigtriangledown$), Pd (khaki solid $\triangleleft$), rare-earth (green solid $\diamondsuit$), Pt (blue open square), Ac (brown solid $\circ$) (**a**) and functions $\lg|\mathrm{e}_4(\sigma_4)|$ (red solid and open $\bigtriangledown$), $\lg \mathrm{d}_{4p1/2}(\sigma_4)$ (green solid and open $\diamondsuit$), $\lg \mathrm{d}_{4p3/2}(\sigma_4)$ (blue solid and open $\bigtriangleup$). Solid symbols are experimental data [3], open ones are theoretic RLDA data [11] (**b**).

above required a separate consideration of the rare-earth elements, which was carried out for all shells in [10].

All the experimental data available in [3] for the P shell and the corresponding theoretical RLDA-results are shown in figure 5. The theoretical points, in contrast to the experimental ones, form rather smooth curves. Note here that the disruptions in d_{6pj} curve repeat the deviations in $\lg|\mathrm{e}_6|$ curve due to the relation (2).

Figure 6 shows the functions d_{nlj} for electronic states with $l = 2, 3$ in $M(n = 3)$, $N(n = 4)$, $O(n = 5)$ shells. First, it is clearly seen that the influence of the spin-orbital interaction on these electronic states is far less than on p states ($l = 1$). Second, a constant difference of the $4dj$-curves in the upper part and their coincidence in the middle part seem to indicate measurement errors.

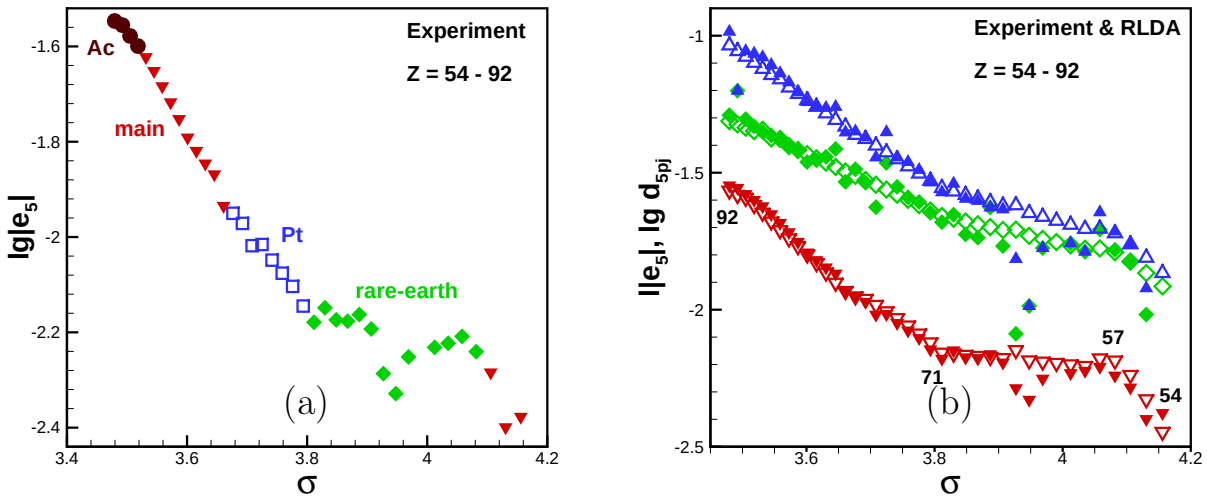

Fig. 4: The function $\lg|\mathrm{e}_5(\sigma_5)|$ for the different atomic groups, denoted by different colors and symbols: main (red solid $\bigtriangledown$), rare-earth (green solid $\diamondsuit$), Pt (blue open square), Ac (brown solid $\circ$) (**a**) and functions $\lg|\mathrm{e}_5(\sigma_5)|$ (red open and solid $\bigtriangledown$), $\lg \mathrm{d}_{5p1/2}(\sigma_5)$ (green open and solid $\diamondsuit$), $\lg \mathrm{d}_{5p3/2}(\sigma_5)$ (blue open and solid $\bigtriangleup$). Solid symbols are experimental data [3], open ones are theoretic RLDA data [11] (**b**).

4 Recovering missing or erroneous electron binding energies

The above analysis of the binding energies from the experimental data [3] found certain patterns. It is assumed that the violation of the patterns in most cases is associated with measurement errors. This section provides examples of recovering missing or questionable measurement results using the found patterns.

The patterns are expressed in smooth dependence of the reduced quantities $\lg|\mathrm{e}_n(\sigma_n)|$ and $\lg \mathrm{d}_{nlj}(\sigma_n)$ which allow their approximation by qubic polynomials:

$$\lg|\mathrm{e}_n(\sigma_n)| = \sum_{k=0}^{3} a_k^{(n)} \sigma_n^k, \qquad \lg \mathrm{d}_{nlj}(\sigma_n) = \sum_{k=0}^{3} b_k^{(nlj)} \sigma_n^k. \tag{3}$$

The coefficients $a_k^{(n)}$ and $b_k^{(nlj)}$ for certain subshells n, l, j within various Z-ranges are presented in table 1 (see section 6).

One can estimate the orbital binding energies (in atomic units) using the

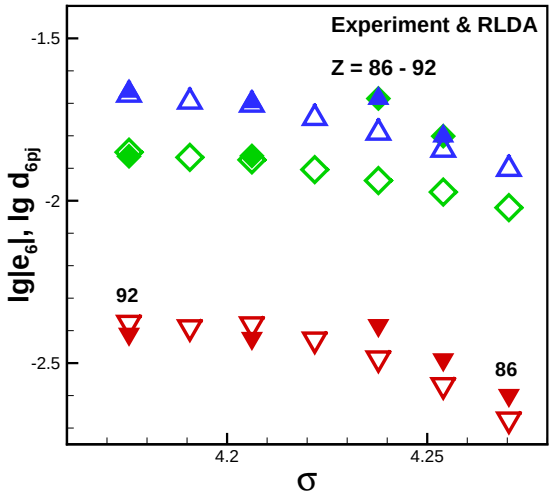

Fig. 5: The functions $\lg|\mathrm{e}_6(\sigma_6)|$ and $\lg \mathrm{d}_{6pj}(\sigma_6)$ from the experimental [3] (solid symbols) and RLDA [11] (open symbols) data: $\lg|\mathrm{e}_6(\sigma_6)|$ (red $\bigtriangledown$), $\lg \mathrm{d}_{6p1/2}(\sigma_6)$ (green $\diamondsuit$), $\lg \mathrm{d}_{6p3/2}(\sigma_6)$ (blue $\bigtriangleup$).

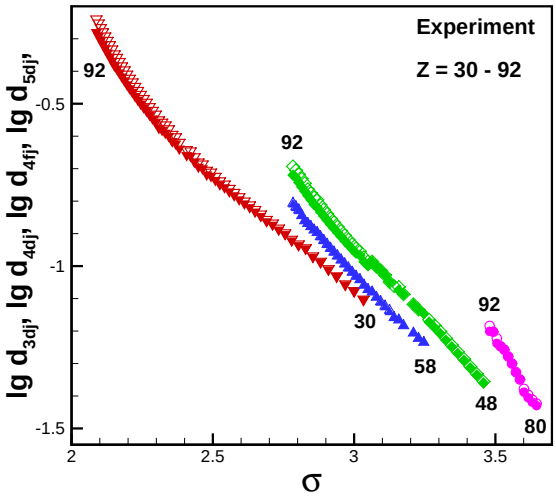

Fig. 6: The functions $\mathrm{d}_{nlj}(\sigma_n)$ for $n = 3,4,5; l = 2,3$ from experimental data [3]. Solid symbols are for $j = l - 1/2$, open ones are for $j = l + 1/2$: $\lg|\mathrm{d}_{3dj}(\sigma_3)|$ (red $\bigtriangledown$), $\lg \mathrm{d}_{4dj}(\sigma_4)$ (green $\diamondsuit$), $\lg \mathrm{d}_{4fj}(\sigma_4)$ (blue $\bigtriangleup$), $\lg \mathrm{d}_{5dj}(\sigma_5)$ (pink $\circ$).

inverse relations to equation (1), (2):

$$E_{n0} = Z^{4/3}\mathrm{e}_n(\sigma_n), \qquad \text{if} \quad l = 0; \qquad \sigma_n = \pi n Z^{-1/3}. \tag{4}$$

$$E_{nlj}(Z) = Z^{4/3}\mathrm{e}_n(\sigma_n) + Z^{2/3}\mathrm{d}_{nlj}(\sigma_n)\lambda^2, \qquad \lambda = l + 1/2, \qquad \text{if} \quad l > 0. \tag{5}$$

and the function interpolations (3) with coefficients from table 1.

In table 2 (see section 6) some estimated energies are shown in comparison with experimental results from the different database [3, 4, 5]. In particular, the error of energy E_{1s} estimates for the light atoms $2 \le Z \le 10$ is within 1-2%, table 2 provides a comparison for $Z = 2, 5, 10$.

The polynomial $\lg|\mathrm{e}_2|$ and $\lg|\mathrm{d}_{2pj}|$ interpolation in the range $10 \le Z \le 23$ are used to correct $2s$ and $2pj$ electron energies in the atoms $_{15}$P and $_{16}$S from [3] and restore missing value for $_9$F. The estimates agree well with the data from the database [4].

The polynomial interpolations of the data in various Z-ranges give a good fit with an inaccuracy less one percent for the $3s$ and $3pj$ energies. The corrected

energies for atom $_{31}$Ga are presented in table 2 with estimates of $4s$ and $5s$ energies for atoms $_{48}$Cd, $_{76}$Os, $_{83}$Bi, $_{85}$At. The corrected energy for osmium is in good agreement with the value from the database [5].

5 Conclusion

The paper analyzes the experimental orbital binding energies in all natural elements from hydrogen to uranium, presented in the table [3]. For each subshell $\{n, l, j\}$, n = 1–6, the dependence of the orbital energies on the atomic number is expressed in terms of a pair of functions $\mathrm{e}_n(\sigma_n)$ and $\mathrm{d}_{nlj}(\sigma_n)$ according to algorithm (1), (2). The continuity of these functions means the existence of an atomic number similarity law of the electronic binding energies in each individual subshell in atoms. This law is semi-empirical in nature, since it was discovered from the analysis of experimental data, but the corresponding dependence on the atomic number is taken from the Thomas–Fermi model.

The degree of smoothness of the functions $\mathrm{e}_n(\sigma_n)$ and $\mathrm{d}_{nlj}(\sigma_n)$ allows one to conclude about both the nature of the filling of the subshells and possible measurement errors. In particular, it is shown that the presence of a bend on the curve $\lg|\mathrm{e}_n(\sigma)|$ associates with filling a new subshell in the corresponding atomic group. In this case, falling out of the general dependence may also indicate a violation of the regular order of filling this subshell.

The established accuracy of the law implementation is 1–2%. It may be used to approximate the experimental binding energies, makes it possible to restore missing and correct erroneous measurements.

A similar analysis of the orbital binding energies calculated by the relativistic local density functional (RLDA) method [2] confirmed the smoothness of the corresponding functions $\lg|\mathrm{e}_n(\sigma_n)|$ and the reasons for their bends, as well as the loss of points from the general dependence upon failure in the order of filling the subshell. Comparison of the results of this model with experimental data shows that its accuracy increases with increasing atomic number, but remains far from spectroscopic one, in contrast to the MCDF model [1].

6 Tables

Table 1: Polynomial coefficients in equation (3).

Z	k	0	1	2	3
	$a_k^{(n)}$, $b_k^{(nlj)}$				
$2 \leq Z \leq 10$	$a_k^{(1)}$	-0.892662	2.897579	-2.042613	0.381917
$10 \leq Z \leq 23$	$a_k^{(2)}$	-6.664277	8.348604	-3.438796	0.422235
	$b_k^{(2p1/2)}$	0.478246	-0.890866	0.294542	-0.056753
	$b_k^{(2p3/2)}$	2.802431	-3.358480	1.172388	-0.161329
$29 \leq Z \leq 92$	$a_k^{(3)}$	6.770856	-7.418470	2.708057	-0.374312
	$b_k^{(3p1/2)}$	5.919896	-6.783210	2.413608	-0.309328
	$b_k^{(3p3/2)}$	21.415101	-22.179422	7.566332	-0.889071
$47 \leq Z \leq 56$	$a_k^{(4)}$	71.437968	-60.264421	16.984158	-1.639032
$71 \leq Z \leq 92$	$a_k^{(4)}$	9.865444	-5.870459	0.592445	0.046382
$71 \leq Z \leq 78$	$a_k^{(5)}$	-26.904410	14.905070	-2.208254	0.000000
$80 \leq Z \leq 88$	$a_k^{(5)}$	57.380454	-30.726296	3.969991	0.000000

Table 2: Orbital binding energies $|E_{nlj}|$ (eV) estimated by Eq.(5) in comparison with experimental data from [3, 4, 5].

Z	n	lj	Eq.(5)	[3]	[4]	[5]
2	1	s	24.52	24.6		24.59
5	1	s	186.8	188.0	186.4–187.3	192.2
9	1	s	703.2	696.7	684.0–694.0	692.4
9	2	s	33.24		23.70–33.64	37.21
15	2	s	186.3	189.0	187.7–188.0	191.4
		p 1/2	129.7	136.0	130.3	135.1[a]
		p 3/2	128.9	135.0	129.4–130.9	
16	2	s	228.3	231.0	229.2	232.1
		p 1/2	166.0	164.0	162.0–166.1	168.1[a]
		p 3/2	164.3	162.0	162.9–164.8	
31	3	s	160.1	159.5	161.0	161.0
		p 1/2	107.4	103.5	106.1–108.7	107.1[a]
		p 3/2	103.9	100.0	104.3–105.8	
48	4	s	109.4	109.8	109.8	112.4
83	4	s	939.5	939.0	939.0	940.8
76	5	s	87.84	84.0	94.6	87.1
85	5	s	193.2	195.0		194.7

[a]Excluding spin-orbit splitting.

7 References

[1] Desclaux J. P. A Multiconfiguration relativistic Dirac-Fock program //Comput. Phys. Commun. **9**, 31 (1975)

[2] Kotochigova S., Levine Z.H., Shirley E.L., Stiles M.D. and Clark C.W. Local-density-functional calculations of the energy of atoms //Phys. Rev. A **55**, 191 (1997)

[3] X-RAY DATA BOOKLET, Center for X-ray Optics and Advanced Light Source Lawrence Berkeley National Laboratory, UPDATE October 2009. – URL: http://xdb.lbl.gov/

[4] NIST X-ray photoelectron spectroscopy database. – URL: https://srdata.nist.gov/xps/selEnergyType.aspx

[5] Thomas D. Binding Energies of Electrons in Atoms from H (Z=1) to Lw (Z=103). – URL: http://www.chembio.uoguelph.ca/educmat/atomdata/bindener/elecbind.html

[6] Deslattes R. D., Kessler E. G. Jr, Indelicato P., de Billy L., Lindroth E. and Anton J. X-ray transition energies: new approach to a comprehensive evaluation //Rev. Mod. Phys. **75**, 35 (2003)

[7] Shpatakovskaya G. V. Semiclassical Method of Analysis and Estimation of the Orbital Binding Energies in Multielectron Atoms and Ions. //Phys. Usp. **62** 186 (2019)

[8] Shpatakovskaya G. V. Atomic-Number Similarity of the K and L x-Ray Terms in Multielectron Atoms //JETP Lett. **108**, 768 (2018)

[9] Shpatakovskaya G. V. Characteristics of the Mearured First Ionization Potentials of Lantanides and Actinides //JETP Lett. **111**, 463 (2020)

[10] Shpatakovskaya G. V. Binding Energies in Electron Shells of Rare-Earth Atoms //JETP **131**, 385 (2020)

[11] Atomic reference data for electronic structure calculation, atomic total energies and eigenvalues. – URL: http://www.nist.gov/pml/data/dftdata/index.cfm

Contents